The Impact of Multivalent Counterions, Al3+, on the Surface Adsorption and Self-Assembly of the Anionic Surfactant Alkyloxyethylene Sulfate and Anionic/Nonionic Surfactant Mixtures

ARTICLE *in* LANGMUIR · OCTOBER 2010

Impact Factor: 4.46 · DOI: 10.1021/la1021356 · Source: PubMed

8 AUTHORS, INCLUDING:

Jordan T Petkov
Unilever
64 PUBLICATIONS **919** CITATIONS
SEE PROFILE

Jeffrey Penfold
University of Oxford
532 PUBLICATIONS **13,301** CITATIONS
SEE PROFILE

Dimiter Petsev
University of New Mexico
96 PUBLICATIONS **2,772** CITATIONS
SEE PROFILE

Isabelle Grillo
Institut Laue-Langevin
142 PUBLICATIONS **2,530** CITATIONS
SEE PROFILE

Langmuir
Article
pubs.acs.org/Langmuir

The Impact of Multivalent Counterions, Al^{3+}, on the Surface Adsorption and Self-Assembly of the Anionic Surfactant Alkyloxyethylene Sulfate and Anionic/Nonionic Surfactant Mixtures

Jordan T. Petkov,[†] Ian M. Tucker,[†] Jeff Penfold,*[,‡,§] Robert K. Thomas,[§] Dimiter N. Petsev,[∥] Chu C. Dong,[§] Steve Golding,[†] and Isabelle Grillo[⊥]

[†]*Unilever Research and Development Laboratory, Port Sunlight, Quarry Road East, Bebington, Wirral, United Kingdom,* [‡]*STFC, Rutherford Appleton Laboratory, Chilton, Didcot, OXON, United Kingdom,* [§]*Physical and Theoretical Chemistry Laboratory, University of Oxford, South Parks Road, Oxford, United Kingdom,* [∥]*Department of Chemical and Nuclear Engineering, MSC01 1120, University of New Mexico, 209 Ferris Engineering Centre, Albuquerque, New Mexico 87131-0001, United States, and* [⊥]*Institute Laue Langevin, 6 Rue Jules Horowitz, F-38042 Grenoble, Cedex 09, France*

Received May 26, 2010. Revised Manuscript Received August 10, 2010

The impact of multivalent counterions, Al^{3+}, on the surface adsorption and self-assembly of the anionic surfactant sodium dodecyl dioxyethylene sulfate, SLES, and the anionic/nonionic surfactant mixtures of SLES and monododecyl dodecaethylene glycol, $C_{12}E_{12}$, has been investigated using neutron reflectivity, NR, and small angle neutron scattering, SANS. The addition of relatively low concentrations of Al^{3+} counterions induces a transition from a monolayer to well-defined surface bilayer, trilayer, and multilayer structures in the adsorption of SLES at the air−water interface. The addition of the nonionic cosurfactant, $C_{12}E_{12}$, partially inhibits the evolution in the surface structure from monolayer to multilayer interfacial structures. This surface phase behavior is strongly dependent upon the surfactant concentration, solution composition, and concentration of Al^{3+} counterions. In solution, the addition of relatively low concentrations of Al^{3+} ions promotes significant micellar growth in SLES and SLES/$C_{12}E_{12}$ mixtures. At the higher counterion concentrations, there is a transition to lamellar structures and ultimately precipitation. The presence of the $C_{12}E_{12}$ nonionic cosurfactant partially suppresses the aggregate growth. The surface and solution behaviors can be explained in terms of the strong binding of the Al^{3+} ions to the SLES headgroup to form surfactant−ion complexes (trimers). These results provide direct evidence of the role of the nonionic cosurfactant in manipulating both the surface and solution behavior. The larger EO_{12} headgroup of the $C_{12}E_{12}$ provides a steric hindrance which disrupts and ultimately prevents the formation of the surfactant−ion complexes. The results provide an important insight into how multivalent counterions can be used to manipulate both solution self-assembly and surface properties.

Introduction

The impact of multivalent counterions on surfactant self-assembly and adsorption is of both fundamental interest and practical importance. In spite of this, it has not been extensively studied, and this is especially true for its impact on surface adsorption. The role and impact of multivalent counterions is of particular importance in the context of the design and performance of products such as detergents and shampoos,[1] and in environmental applications,[2] such as the removal of toxic metals in wastewater treatment and in soil remediation. More recently, it has also been demonstrated that multivalent counterions have potential impact in the manipulation of self-assembly for a range of applications in nanotechnology.[3]

The anionic surfactants such as sodium dodecyl sulfate, SDS, sodium dodecyl benzene sulfonate, SDBS, and sodium dodecyl dioxyethylene sulfate, SLES, are important and widely used surfactants in the context of applications.[4] The impact of monovalent electrolytes, such as NaCl, has been extensively studied,[5,6] where the addition of electrolyte promotes micellar growth, reduces critical micellar concentrations, cmc's, and enhances adsorption. In other related surfactant systems, the addition of aromatic counterions, such as benzoate, salicylate, and tosylate,[7] results in significant micellar growth at low surfactant and counterion concentrations. In these systems, the sensitivity to particular isomeric forms has attracted much attention.[8] Studying the impact of multivalent counterions on surfactants such as SDS has proved difficult, as the addition of such counterions quickly leads to precipitation.[9] This was also discussed by Alargova and co-workers,[10−13] who overcame this by using the alkyloxyethylene surfactant SLES. Here the small oxyethylene group increases the surfactant solubility and suppresses precipitation. As such, anionic

*To whom correspondence should be addressed. E-mail: jeff.penfold@stfc.ac.uk.

(1) Yang, J. *Curr. Opin. Colloid Interface Sci.* **2002**, *7*, 276.
(2) Scamehorn, J. F.; Christian, S. D.; Ellington, R. T. In *Surfactant based separation processes*; Scamehorn, J. F.; Harwell, J. H., Eds.; Surfactant Science Series Volume *33*; Marcell Dekker: New York, 1989.
(3) Piestil, J.; Pospisil, H.; Kriz, J.; Kadlec, P.; Tuzar, Z.; Cubitt, R. *Langmuir* **2001**, *17*, 6699.
(4) *Anionic Surfactants*; Gloxhuber, C., Kunstler, K., Eds.; Surfactant Science Series Volume *43*; Marcell Dekker: New York, 1997.
(5) Penfold, J.; Tucker, I.; Thomas, R. K.; Staples, E.; Schuermann, R. *J. Phys. Chem. B* **2005**, *109*, 10760.
(6) Missel, P. J.; Mazer, N. A.; Carey, M. C.; Benedek, G. B. *J. Phys. Chem.* **1989**, *93*, 8354.
(7) Kreke, P. J.; Magid, L. J.; Gee, J. C. *Langmuir* **1996**, *12*, 699.
(8) Penfold, J.; Tucker, I.; Staples, E.; Thomas, R. K. *Langmuir* **2004**, *20*, 8054.
(9) Stellner, K. L.; Scamehorn, J. F. *J. Am. Oil Chem. Soc.* **1986**, *63*, 566.
(10) Alargova, R. G.; Petkov, J. T.; Petsev, D; Ivanov, I. B.; Broze, G; Mehreteab, A *Langmuir* **1995**, *11*, 1530.
(11) Alargova, R. G.; Danov, K. D.; Petkov, J. T.; Kralchevzsky, P. A.; Broze, G; Mehreteab, A *Langmuir* **1997**, *13*, 5544.
(12) Alargova, R. G.; Danov, K. D.; Kralchevzsky, P. A.; Broze, G; Mehreteab, A *Langmuir* **1998**, *14*, 4036.
(13) Alargova, R. G.; Petkov, J. T.; Petsev, D. N. *J. Colloid Interface Sci.* **2003**, *261*, 1.

surfactants of this general form, with different oxyethylene groups, are now extensively used in many current formulations.[14]

In their pioneering studies, Alargova and co-workers[10−13] have used light scattering and surface tension to explore the effect of multivalent counterions on the micellization and surface properties of the alkyloxyethylene surfactant and its mixtures with nonionic surfactants. From the light scattering measurements, they deduced that the strong binding of Ca^{2+} or Al^{3+} promoted micellar growth at very low ionic strength, compared to monovalent counterions. They correlated this onset of growth with the point at which counterions are in excess, defined by the parameter $\xi < 1.0$ (where $\xi = (C_s - \text{cmc})/z_m C_m$; C_s is the surfactant concentration, cmc the critical micellar concentration, and z_m, C_m are the counterion charge and concentration, respectively). The mechanism was ascribed to surfactant−ion complex formation (dimer or trimer). Furthermore, they showed that in the presence of a nonionic surfactant the micellar growth can be suppressed if the nonionic surfactant headgroup was large enough to hinder that complex formation. The surface tension was shown to decrease with increasing counterion concentration, up to $\xi = 1.0$, and the concentration dependence of the surface tension was explained in terms of ion and counterion adsorption at the interface. However, there was no direct information about the structure and composition of the surface layer.

In a related study, Penfold et al.[15] have investigated the effect of Ca^{2+} on the adsorption at the air−water interface and on the self-assembly of SDBS/$C_{12}E_8$ ($C_{12}E_{23}$) surfactant mixtures using NR and SANS. In particular, they demonstrated that the addition of Ca^{2+} ions at relatively low concentrations induced a transition from globular micelles to planar structures in SDBS and SDBS/$C_{12}E_8$ ($C_{12}E_{23}$) mixtures. This occurred at concentrations where the system was relatively insensitive to monovalent electrolytes such as NaCl. Furthermore, the larger EO headgroup of $C_{12}E_{23}$ provided a more effective steric hindrance to suppress that transition to SBDS richer solution compositions. Most importantly, they were also able to investigate the impact of multivalent counterions on the surface adsorption and on the structure of the adsorbed layer. The addition of Ca^{2+} produced a transition from monolayer to bilayer and ultimately to multilayer structures at the interface. The complex evolution in the surface structure was found to be dependent upon the Ca^{2+} concentration and the SDBS/nonionic surfactant composition. By analogy with the self-assembly behavior, the addition of the cosurfactant suppresses the more complex multilayer structure formation, such that the evolution in the solution and surface structures was highly correlated.

In this paper, we report the use of NR and SANS to study the surface adsorption at the air−water interface and the solution properties of SLES/$C_{12}E_{12}$ mixtures in the presence of $AlCl_3$. The results provide a more direct and detailed quantitative evaluation of the impact of Al^{3+} ions on self-assembly in solution. Furthermore, they provide the first quantified description of the corresponding changes in the surface adsorption at the air−water interface, and in the evolution in the surface structure from a monolayer to multilayer structures at the interface. This provides an important and interesting insight into how to manipulate surface and solution structures in such systems.

Experimental Details

a. Neutron Reflectivity (NR). Specular neutron reflectivity measurements were made on the SURF reflectometer at the ISIS pulsed neutron source at the Rutherford Appleton Laboratory, U.K.[16] The measurements were made using a single detector at a fixed angle, θ, of 1.5° and neutron wavelengths, λ, in the range 0.5−6.8 Å in order to access a Q range (Q is the wave vector transfer normal to the surface, defined as $Q = (4\pi/\lambda)\sin\theta$ where λ is the neutron wavelength and θ is the grazing angle of incidence) of 0.048−0.5 $Å^{-1}$, using what are now well established experimental procedures.[17] The basis of a neutron reflectivity experiment is that the variation in specular reflection, $R(Q)$, with Q is related to the composition or density profile in a direction normal to the interface.

In the kinematic or Born approximation, the reflectivity is related to the square of the Fourier transform of the scattering length density profile, $\rho(z)$, normal to the interface,[18] that is,

$$R(Q) = \frac{16\pi^2}{Q^2}\left|\int \rho(z)\, e^{-iQz}\, dz\right|^2 \quad (1)$$

where $\rho(z) = \Sigma_i n_i(z) b_i$, with $n_i(z)$ being the number density of the ith nucleus and b_i its scattering length. The strength of this technique for studying surfactants adsorbed at interfaces is the ability to substitute deuterium for hydrogen in part or all of the amphiphile. Hence, the scattering length density or neutron refractive index profile (the neutron refractive index is defined as $n = 1 - \lambda^2\rho(z)/2\pi$) can be manipulated without any significant change to the physical properties of the amphiphile. This use of isotopic substitution in combination with NR has been powerfully demonstrated for the study of surfactant adsorption (for the determination of adsorbed amounts and surface structure) in a wide range of surfactants, surfactant mixtures, and polymer−surfactant mixtures.[19] More specifically, at the air/water interface, D/H isotopic substitution can be used to index match the solvent to the air phase (null reflecting water, nrw, 8 vol% D_2O/H_2O mixture, with a refractive index of 1.0 for neutrons) such that the only contribution to the scattering at the interface arises from the deuterated surfactant which is adsorbed at the interface. The reflected signal can be analyzed in terms of the adsorbed amount at the interface and the thickness of the adsorbed layer. The most direct procedure for determining the surface concentration of surfactant is to assume that it is in the form of a single layer of uniform composition. The measured reflectivity can then be fitted by comparing it with a profile calculated using the optical matrix method for this simple structural model.[20] The parameters obtained for such a model fit are the scattering length density, ρ, and the thickness, d, of the layer. The area per molecule is then given by

$$A = \sum_i b_i/\rho d \quad (2)$$

where Σb_i is the scattering length of the adsorbed surfactant molecule.

For the neutron reflectivity data reported here, there are regions of surfactant concentration where the adsorbed layer is well described as a thin monolayer of uniform composition (density), and regions where the surface structure is more complex. In these cases, the simplest model consistent with the data is used to describe the surface structure. Where a pronounced interference fringe is observed, two or three layers are mostly sufficient to describe the data. In cases where a pronounced Bragg peak is observed, indicative that more extensive multilayer

(14) Hossel, P.; Dieing, R.; Norenberg, H.; Pfau, C. J.; Sander, J. *Int. J. Cosmet. Sci.* **2000**, *22*, 1.
(15) Penfold, J.; Thomas, R. K.; Dong, C. C.; Tucker, I.; Metcalfe, K.; Golding, S.; Grillo, I. *Langmuir* **2007**, *23*, 10140.
(16) Penfold, J. *J. Chem. Soc., Faraday Trans.* **1997**, *93*, 3899.
(17) Lee, E. M.; Thomas, R. K.; Penfold, J.; Ward, R. C. *J. Phys. Chem.* **1989**, *93*, 381.
(18) Penfold, J.; Thomas, R. K. *J. Phys.: Condens. Matter* **1990**, *2*, 1369.
(19) Lu, J. R.; Thomas, R. K.; Penfold, J. *Adv. Colloid Interface Sci.* **2000**, *84*, 143.
(20) Penfold, J. In *Neutron, x-ray, and light scattering*; Lindner, P., Zemb, T., Eds.; Elsevier: New York, 1991.

formation is occurring at the air−water interface, a more sophisticated approach is required to evaluate the surface structure.

In the kinematic approximation, and consistent with the approach of Tidswell et al.[21] and Sinha et al.,[22] the specular reflectivity for such a multilayer at the interface can be written as

$$R(Q) = \frac{16\pi^2}{Q^2}\left|\sum_{i=0}^{2N}(\rho_i - \rho_{i+1})\exp(-iQd_i)\exp\left(-Q^2\frac{\sigma_i^2}{2}\right)\right|^2 \quad (3)$$

where ρ_i is the scattering length density of the ith layer, $i = 0$ represents the subphase, d_i is the distance of the interface between the ith and $i+1$th layers from the subphase, $d_i = \Sigma_i l_i$, l_i is the thickness of the ith layer, σ_i is the roughness between the ith and $i+1$th layers, $\rho(2N+1)$ is the upper bulk phase (air), and $2N$ is the number of layers (N is the number of bilayers). The definition of the bilayer structure with increasing depth is modified by an exponential decay constant, such that

$$\rho(i) = \rho_N - \Delta\rho\exp(-d_i/\eta) \quad (4)$$

and η is a damping coefficient.

b. Small Angle Neutron Scattering (SANS). SANS measurements were made both on the LOQ diffractometer[23] at the ISIS pulsed neutron source at the Rutherford Appleton Laboratory, and on the D11 diffractometer[24] at the Institute Laue Langevin, Grenoble, France. The measurements on LOQ were made using the white beam time-of-flight method, in the scattering vector, Q, range of 0.008−0.25 Å^{-1}. The measurements on D11 were made using a wavelength of 6 Å ($\Delta\lambda/\lambda \sim 10\%$) and two different detector distances (2.0 and 5.0 m), to cover the Q range of ∼0.006−0.25 Å^{-1}. The samples were contained in Starna 1 mm path length quartz spectrophotometer cells and maintained at a temperature of 25 °C. The data were corrected for background scattering, detector response, and the spectral distribution of the incident neutron beam, and converted to an absolute scattering cross section ($I(Q)$ in cm^{-1}) using standard procedures.[25,26]

In SANS, the scattering cross section, or scattered intensity, for colloidal aggregates in solution can be written as[27]

$$I(Q) = N\left|\int_v \left(\rho_p(r) - \rho_s\right)\exp iQr d^3r\right|^2 \quad (5)$$

where ρ_p and ρ_s are the aggregate and solvent scattering length densities, respectively, and N is the number of aggregates per unit volume. In the micellar phase, the micelle structure is determined by analyzing the scattering data using a standard and well established model for globular micelles.[28] For a solution of globular polydisperse interacting particles (micelles), the scattered intensity can be written in the "decoupling approximation"[28] as

$$I(Q) = n\left[S(Q)\left|\left\langle F(Q)\right\rangle_Q\right|^2 + \left\langle\left|F(Q)\right|^2\right\rangle_Q - \left|\left\langle F(Q)\right\rangle_Q\right|^2\right] \quad (6)$$

where the averages denoted by $\langle Q\rangle$ are averages over particles size and orientation, n is the micelle number density, $S(Q)$ is the structure factor, and $F(Q)$ is the form factor. The micelle structure (form factor) is modeled using a standard "core and shell" model,[28] where the form factor is

$$F(Q) = V_1(\rho_1 - \rho_2)\,F_0(QR_1) + V_2(\rho_2 - \rho_s)\,F_0(QR_2) \quad (7)$$

and R_1, R_2 are the core and shell radii, $V_i = 4\pi R_i^3/3$, $F_0(QR_i) = 3j_1(QR_i)/(QR) = 3[\sin(QR) - QR\cos(QR)]/(QR)^3$, ρ_1, ρ_2, and ρ_s are the scattering length densities of the micelle core and shell, and of the solvent, respectively, and $j_1(QR_i)$ is a first order spherical Bessel function.

The micelle core + shell model[28] comprises an inner core made up of the alkyl chains only and constrained to space fill a volume limited by a radius, R_1, limited to the fully extended chain length of the surfactant, l_c. For larger aggregation numbers, ν, volumes greater than that defined by R_1 (as is found in this study) are accommodated by a prolate elliptical distortion with dimensions R_1, R_1, eeR_1 (where ee is the elliptical ratio). The outer shell, of dimensions R_2, R_2, eeR_2, contains the headgroups and the corresponding hydration water. Representative hydration values for the headgroup and the bound counterions are included as fixed values, and the modeling is not particularly sensitive to variations in hydration. From the known molecular volumes and neutron scattering lengths, the scattering length density (ρ) for the core, shell, and solvent can be estimated.[29] An additional model parameter, ext, is included to accommodate departures from the relatively simple packing constraints and assumed partial molar volumes, and it has been discussed in detail elsewhere.[30,31] For the mixed systems, the two surfactant components in the binary mixture are accommodated by assuming ideal mixing, which has been shown to be consistent with previous observations for concentrations well in excess of the mixed cmc.[32] The interparticle interactions are included using the rescaled mean spherical approximation, RMSA, calculated for a repulsive screened Coulombic potential,[33,34] defined by the surface charge, z, the micelle number density, n, the micelle diameter, and the Debye−Huckel inverse screening length, κ^{-1}.[35] The model parameters refined are then ν, z, and ee, and an accepTable model fit requires the shape of the scattering to be reproduced and the absolute value of the scattered intensity to be predicted to within ±10%.

c. Materials and Measurements Made. The alkyl chain deuterated SLES (d-SLES) and hydrogeneous SLES (h-SLES) were synthesized by Oxford/Unilever Research and Development[36] and purified using well established procedures. The purity and consistency of the d- and h-SLES were confirmed by NR. The h-$C_{12}E_{12}$ was obtained from Nikkol and used without further purification. All the solutions for the SANS measurements were made in D_2O, which was obtained from Fluorochem. The solutions for the neutron reflectivity measurements were made in nrw, and high purity water (Elga Ultrapure) was used with the D_2O. Analytical grade (>99.9% purity) NaCl, $CaCl_2$, and $AlCl_3$ were used for the solutions in electrolyte. All glassware and sample cells were cleaned using alkali detergent (Decon 90), followed by copious washing in high purity water.

SANS measurements were made for 20 mM SLES and 20 mM 95:5, 90:10, and 80:20 mol ratio SLES/$C_{12}E_{12}$ in NaCl, NaCl/$CaCl_2$, and NaCl/$AlCl_3$ electrolyte (where the combinations of

(21) Tidswell, I. M.; Ocko, B. M.; Pershan, P. S.; Wasserman, S. R.; Whitesides, G. M.; Axe, J. D. *Phys. Rev. B* **1990**, *41*, 1111.
(22) Sinha, S. K.; Sanyal, M. K.; Satija, S. K.; Majkrzak, C. F.; Neumann, D. A.; Homma, H.; Szpala, S.; Gibaud, H.; Morkov, H. *Phys. B* **1994**, *198*, 72.
(23) Heenan, R. K.; King, S. M.; Penfold, J. *J. Appl. Crystallogr.* **1997**, *30*, 1140.
(24) Neutron beam facilities at the high flux reactor available for users, ILL, Grenoble France, 1994.
(25) Heenan, R. K.; King, S. M.; Osborn, R.; Stanley, H. B. RAL Internal Report, RAL-89-128, 1989.
(26) Ghosh, R. E.; Egelhaaf, S. U.; Rennie, A. R. ILL Internal Report, ILL 98GH14T, 1998.
(27) Penfold, J. Neutron scattering studies of micellar structure. *Encylopedia of Surface and Colloid Science*; Somasundaran, P., Hubbard, J., Eds.; Marcell Dekker: New York, 2002; p 3653.
(28) Hayter, J. B.; Penfold, J. *Colloid Polym. Sci.* **1983**, *261*, 1032.
(29) Tanford, C. *J. Phys. Chem.* **1972**, *76*, 3020.
(30) Penfold, J.; Staples, E.; Ugazio, S.; Tucker, I.; Soubiran, L.; Hubbard, J.; Noro, M.; O'Malley, B.; Ferrante, A.; Buron, H. *J. Phys. Chem. B* **2005**, *109*, 18107.
(31) Penfold, J.; Staples, E.; Tucker, I.; Thomas, R. K. *Langmuir* **2004**, *20*, 1269.
(32) Staples, E.; Penfold, J.; Thompson, L.; Tucker, I.; Hubbard, J.; Thomas, R. K.; Lu, J. R. *Langmuir* **1995**, *11*, 2479.
(33) Hayter, J. B.; Penfold, J. *Mol. Phys.* **1981**, *42*, 109.
(34) Hayter, J. B.; Hansen, J. P. *Mol. Phys.* **1982**, *42*, 651.
(35) Hayter, J. B.; Hansen, J. P. ILL Int Sci Rep 84HA14T, 1982.
(36) Thomas, R. K.; Dong, C. C.; Golding, S.; Gibson, C. Private communication.

electrolytes were adjusted to maintain constant ionic strength). Further SANS measurements were made for 5 mM SLES and 95:5, 93.5:6.5, and 90:10 mol ratio SLES/$C_{12}E_{12}$ in NaCl/$CaCl_2$ and NaCl/$AlCl_3$ mixtures. All the SANS measurements were made in D_2O using hydrogeneous surfactants to provide maximum contrast and sensitivity.

Neutron reflectivity measurements were made in nrw, using d-SLES and d-SLES/h-$C_{12}E_{12}$ for the SLES/$C_{12}E_{12}$ mixtures. Measurements for d-SLES in nrw were made in the concentration range $3 \times 10^{-6}-5 \times 10^{-3}$ M, and for d-SLES and 50:50 mol ratio d-SLES/h-SLES for $c >$ cmc to characterize the adsorption isotherm of SLES and to verify its purity. Measurements were made for 1 and 5 mM d-SLES and d-SLES/h-$C_{12}E_{12}$ mixtures at SLES/$C_{12}E_{12}$ mole ratios of 90:10, 92:8, 93.5:6.5, and 95:5 (at 5 mM) and 90:10 and 95:5 (at 1 mM) in NaCl/$AlCl_3$ mixtures. Some additional measurements, but of limited scope, were made in NaCl/$CaCl_2$ mixtures. Finally, some limited measurements were made d-SLES at 5 mM in NaCl/$CaCl_2$ and NaCl/$AlCl_3$, where the electrolyte was added to the initial solution or added after the solution had been transferred to the reflectivity troughs. All the reflectivity measurements were made at 25 °C.

Results and Discussion

a. Small Angle Scattering. The small angle scattering data for 20 mM SLES in $AlCl_3$/NaCl and $CaCl_2$/NaCl mixed electrolytes for increasing $AlCl_3$ and $CaCl_2$ concentrations are shown in Figure 1. At the lowest $AlCl_3$ and $CaCl_2$ concentrations, the data are consistent with the formation of small globular micelles. With increasing $AlCl_3$ and $CaCl_2$ concentration, the increase in the scattering at low Q values is consistent with micellar growth.

The solid lines are model fits for the core−shell model for globular interacting micelles, as described earlier, and the key model parameters are summarized in Table 1. The scattering is largely dominated by the form factor, and the model provides a good description of the data.

Also summarized in Table 1a are the key model parameters from the core−shell model for 20 mM SLES in NaCl (the data are broadly similar to the data shown in Figure 1, and are not displayed here).

For 20 mM SLES, the micelle aggregation number, v, is ∼90, the degree of ionization, δ, is ∼0.17, and the micelles are slightly elliptical with an axial ratio of ∼1.3. With the addition of NaCl, there is some modest micellar growth. In 144 mM NaCl, the aggregation number is ∼150, and the axial ratio is ∼1.7. Correspondingly, the surface charge on the micelles has decreased to almost zero. For the addition of $CaCl_2$ and $AlCl_3$, the micellar growth with increasing $CaCl_2$ and $AlCl_3$ concentration is significantly more pronounced. For the addition of $CaCl_2$, the micelle aggregation number increases from ∼160 at 4.8 mM $CaCl_2$ to ∼570 at 24 mM $CaCl_2$, the corresponding axial ratio increases from 1.6 to 5.6, and the surface charge rapidly decreases to zero. For the addition of $AlCl_3$, the micelle aggregation number increases from ∼130 to ∼1200, and the ellipticity increases from 1.4 to 13.0 as the $AlCl_3$ concentration increases from 0.0 to 7.8 mM. The surface charge decreases rapidly to zero with increasing $AlCl_3$ concentration, as was observed with the addition of $CaCl_2$.

Similar SANS measurements were made at the same solution concentration but for different SLES/$C_{12}E_{12}$ mixture compositions. The measurements were made at solution compositions of 95/5 and 90/10 mol ratio SLES/$C_{12}E_{12}$ and for the addition of $CaCl_2$/NaCl. Measurements were also made for the addition of $AlCl_3$/NaCl over a wider range of SLES/$C_{12}E_{12}$ compositions, 95/5, 90/10, and 80/20 mol ratio SLES/$C_{12}E_{12}$. The data are also all consistent with the formation of globular micelles, whose size depends upon the SLES/$C_{12}E_{12}$ composition, the electrolyte type and concentration. The data were all modeled using the micellar core−shell model, and the key model parameters are summarized in Table S1 in the Supporting Information.

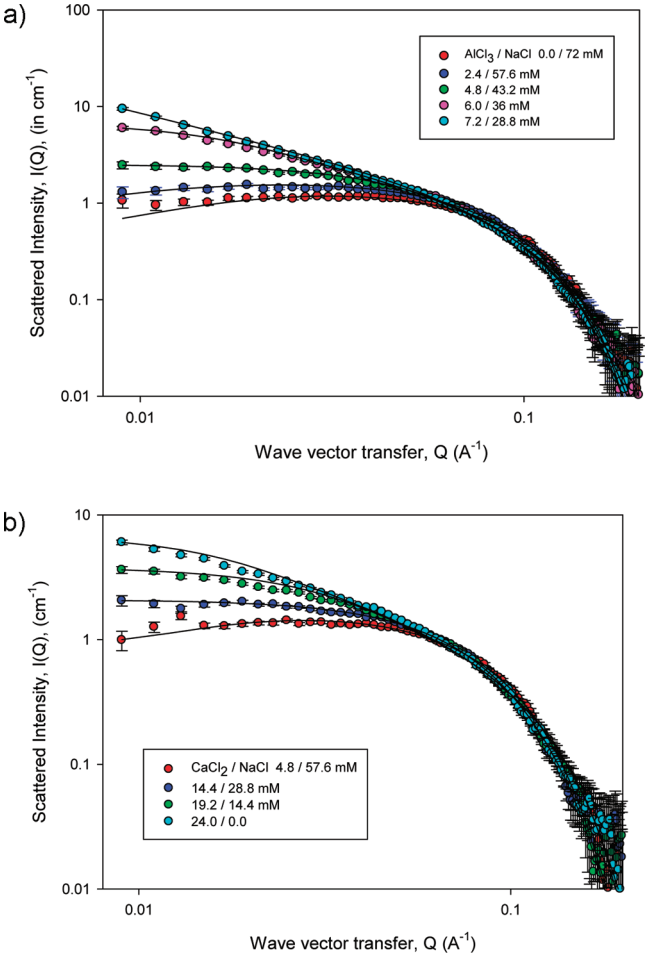

Figure 1. (a) Scattered Intensity, $I(Q)$, for 20 mM SLES/$AlCl_3$/NaCl for different $AlCl_3$/NaCl concentrations. $AlCl_3$/NaCl (see legend). (b) Scattered Intensity, $I(Q)$, for 20 mM SLES/$CaCl_2$/NaCl for different $CaCl_2$/NaCl concentrations (see legend). The solid lines are model fits as described in the text.

At the surfactant concentration of 20 mM and at 5 mM in the purely micellar region, the data have been quantified using the same core−shell model for globular micelles. The micelle growth/elongation is accommodated by assuming ellipsoids of increasing anisotropy. For much of the data, the finite Q range ($Q_{min} \sim$ 0.006−0.008 Å^{-1}) is adequate for a reliable evaluation of the model parameters. However, in the regions of more extreme growth, the finite Q range introduces a greater uncertainty in the evaluation of the actual micelle size, and the errors in the quoted aggregation numbers reflect that greater uncertainty.

Further SANS measurements were made at a lower surfactant concentration of 5 mM, for SLES and different SLES/$C_{12}E_{12}$ mixtures (at solution compositions of 93.5/6.5, 95/5, and 90/10 mol ratio), and for the addition of $AlCl_3$/NaCl mixed electrolyte. Some typical SANS data, measured at the solution concentration of 5 mM, are shown in Figure 2.

In Figure 2a, the scattering data for 5 mM SLES and for $AlCl_3$ concentrations from 0.6 to 1.8 mM are shown. At the lower $AlCl_3$ concentrations, the data are consistent with globular micelles, and there is micellar growth with increasing $AlCl_3$ concentration. At the highest $AlCl_3$ concentration illustrated (1.8 mM), the form of the data is different. There is now a Q^{-2} dependence at the low Q

Table 1

(a) Micelle Model Parameters for 20 mM SLES/NaCl

NaCl conc (mM)	aggregation number, v	charge, z (±1)	R_1 (±1 Å)	R_2 (±1 Å)	ee (±0.1)	ext (±0.05)
0.0	90 ± 5	15	17	21	1.3	1.05
18	109	7	17	21	1.4	1.05
36	120 ± 7	5	18	22	1.5	1.1
54	127	4	19	23	1.4	1.15
72	132	4	19	23	1.5	1.15
144	153 ± 10	3	19	23	1.7	1.15

(b) Micelle Model Parameters for 20 mM SLES/$CaCl_2$/NaCl

$CaCl_2$/NaCl conc(mM)	aggregation number, v	charge, z (±1)	R_1 (±1 Å)	R_2 (±1 Å)	ee (±0.1)	ext (±0.05)
4.8/57.6	160 ± 10	4	20	24	1.6	1.2
9.6/43	179	2	20	24	1.8	1.2
12.0/36	191 ± 15	1	20	24	1.8	1.2
14.4/28.8	213	0	20	24	2.0	1.2
19.2/14.4	359 ± 20	0	20	24	3.5 ± 0.2	1.2
24.0/0.0	573 ± 40	0	20	24	5.6 ± 0.5	1.2

(c) Micelle Model Parameters for 20 mM SLES/$AlCl_3$/NaCl

$AlCl_3$/NaCl conc(mM)	aggregation number, v	charge, z (±1)	R_1 (±1 Å)	R_2 (±1 Å)	ee (±0.1)	ext (±0.05)
0.0/72	132 ± 7	4	20	24	1.4	1.2
2.4/57.6	169 ± 15	3	20	24	1.7	1.2
4.8/43.2	260 ± 20	0	20	24	2.7	1.2
6.0/36	578 ± 40	0	20	24	5.9 ± 0.5	1.2
7.2/28.8	945 ± 70	0	20	24	9.6 ± 1	1.2
7.5/27	1084 ± 100	0	20	24	11.1 ± 1	1.2
7.8/25	1232 ± 100	0	20	24	12.6 ± 1	1.2

values and the formation of a Bragg peak at high Q (~0.12 $Å^{-1}$). There are features that are consistent with the formation of multilamellar structures, and the microstructure is in the form of micellar/lamellar coexistence. At even higher $AlCl_3$ concentrations (data not shown), the lamellar component increases further and eventually precipitation occurs. The scattering data in Figure 2b for 5 mM 95/5 mol ratio SLES/$C_{12}E_{12}$ and for the addition of $AlCl_3$/NaCl mixtures show a similar trend with increasing $AlCl_3$ concentration. The difference is that the micellar growth and the onset of multilamellar formation is now shifted to higher $AlCl_3$ concentrations. This is again consistent with the hindrance of SLES/Al^{3+} complex formation by the bulky EO_{12} headgroup of the $C_{12}E_{12}$ cosurfactant. The scattering data at 5 mM in the predominantly micellar region were analyzed quantitatively using the core−shell micellar model described earlier, and the key model parameters are summarized in Table S2 in the Supporting Information. The transition from micellar to micellar/lamellar coexistence, as illustrated in Figure 2, is broadly similar to that reported for related systems. In the SDBS/$C_{12}E_8$[15] and SDBS/triethylene glycol decyl ether, $C_{10}E_3$,[37] surfactant mixtures, the addition of Ca^{2+} promoted a similar transition.

Alargova and co-workers[10−13] deduced from their light scattering data that the strong binding of Ca^{2+} and Al^{3+} to the SLES induced significant micellar growth when the parameter ξ was < 1.0, that is, when the counterions were in excess. From the neutron scattering measurements, we have been able to provide a more detailed and precise quantification of that micellar growth. In Figure 3, the variation in the micelle aggregation number with ξ is plotted for 20 mM SLES in $AlCl_3$/NaCl and $CaCl_2$/NaCl mixtures (Figure 3a), for 20 mM SLES/$C_{12}E_{12}$ mixtures in $AlCl_3$/NaCl mixed electrolyte (Figure 3b), and for 20 mM SLES/$C_{12}E_{12}$ mixture in $CaCl_2$/NaCl mixed electrolyte (Figure 3c).

(37) Tucker, I.; Penfold, J.; Thomas, R. K.; Dong, C. C.; Golding, S.; Gibson, S.; Grillo, I. *Langmuir* **2010**, *26*, 10614.

In Figure 3a for 20 mM SLES, it is observed that, consistent with the observations of Alargova and co-workers,[10−13] the onset of significant micellar growth occurs at $\xi \sim 1.0$. Furthermore, the micelle growth is substantially more pronounced in the presence of Al^{3+} than in Ca^{2+}. This is consistent with a stronger complexation between the SLES and Al^{3+} than with Ca^{2+}. Significantly, the addition of up to 24 mM NaCl resulted in only a relatively modest increase in the micelle aggregation number (from ~90 in the absence of electrolyte to ~150 in 24 mM NaCl; see Table 1a).

In Figure 3b and c, the impact of the nonionic cosurfactant, $C_{12}E_{12}$, in disrupting the complex formation and suppressing micellar growth is illustrated. In Figure 3b, it is demonstrated that increasing the amount of $C_{12}E_{12}$ present increasingly reduces the SLES/Al^{3+} complex formation and hence micellar growth, due to the steric hindrance of the bulky EO_{12} headgroup. Alargova and co-workers[10−13] observed that the addiiton of $C_{12}E_4$, with its much smaller headgroup and a tendency to form more planar structures, did not result in the same reduction compared to $C_{12}E_{10}$. At 5 mol % $C_{12}E_{12}$, the effect is relatively modest, but when the $C_{12}E_{12}$ composition has increased to 20 mol %, the impact of the Al^{3+} counterions has been almost completely suppressed. In contrast, in the presence of $CaCl_2$, the addition of $C_{12}E_{12}$ has a much more immediate impact. With only 5 mol % $C_{12}E_{12}$, the micellar growth with increasing Ca^{2+} concentration is almost completely suppressed.

The strong binding of the Al^{3+} and Ca^{2+} counterions to the micellar surface reduces the local curvature and promotes micellar growth. The effect is more pronounced for Al^{3+} than Ca^{2+} where SLES/Al^{3+} trimers are formed, compared to the formation of SLES/Ca^{2+} dimers. The addition of the nonionic cosurfactant with a large headgroup, $C_{12}E_{12}$, suppresses the dimer/timer formation due to the steric hindrance of the EO_{12} headgroup. This disruption appears to be more effective in the presence of Ca^{2+} than Al^{3+}, and this is also an indication of the relative strength of the respective interactions.

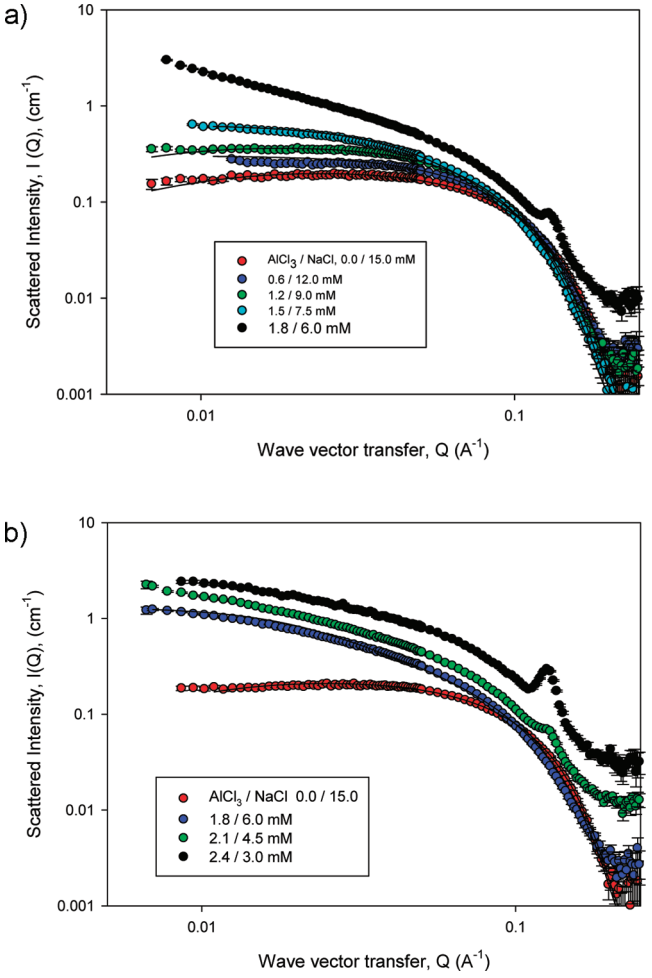

Figure 2. (a) Scattered intensity, $I(Q)$, for 5 mM SLES/$AlCl_3$/NaCl for different $AlCl_3$/NaCl concentrations (see legend); data for (black solid circle) 1.8/6.0 mM $AlCl_3$/NaCl shifted vertically for clarity. (b) Scattered intensity, $I(Q)$, for 5 mM 95/5 mol ratio SLES/$C_{12}E_{12}$/$AlCl_3$/NaCl for different $AlCl_3$/NaCl concentrations (see caption); the data (green solid circle) for 2.1/4.5 mM and (solid black circle) 2.4/3.0 mM $AlCl_3$/NaCl are shifted vertically for clarity. The solid lines are model fits as described in the text.

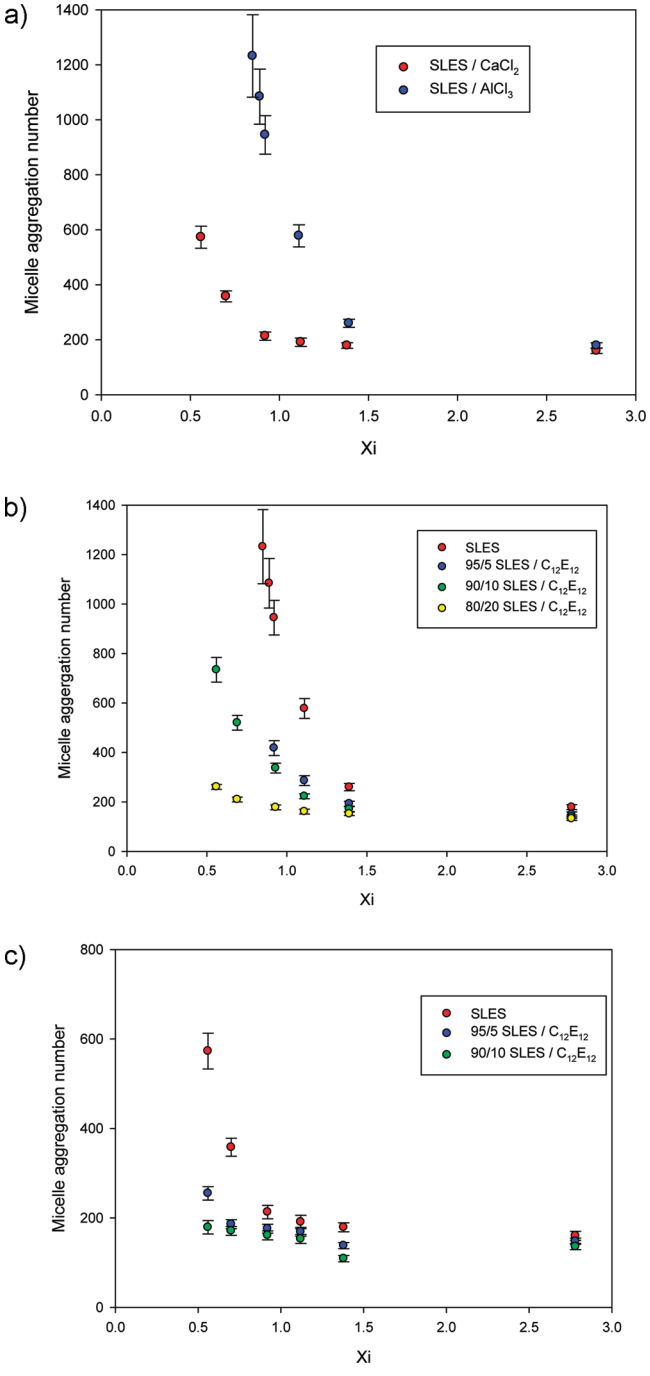

Figure 3. (a) Variation in micelle aggregation number with ξ for 20 mM SLES in (blue solid circle) $AlCl_3$/NaCl and (black solid circle) $CaCl_2$/NaCl. (b) Variation in micelle aggregation number with ξ for 20 mM SLES/$C_{12}E_{12}$ in $AlCl_3$/NaCl, (red solid circle) SLES, (blue solid circle) 95/5 mol ratio SLES/$C_{12}E_{12}$, (green solid circle) 90/10, and (yellow solid circle) 80/20. (c) Variation in micelle aggregation number with ξ, for 20 mM SLES/$C_{12}E_{12}$ in $CaCl_2$/NaCl, (red solid circle) SLES, (blue solid circle) 95/5 mol ratio SLES/$C_{12}E_{12}$, and (green solid circle) 90/10.

Here the impact of the addition of the nonionic cosurfactants is to reduce the strong SLES/multivalent counterion complex formation, which drives the trend toward larger aggregates with reduced local curvature. The steric hindrance of the lager EO_{12} headgroup disrupts the dimer/trimer formation. This is in contrast to what is normally encountered in ionic/nonionic surfactant mixtures, where the addition of a nonionic cosurfactant promotes micellar growth by reducing the electrostatic interaction between the ionic headgroups and the electrostatic contribution to the free energy of micellization. This has been discussed in detail elsewhere, for example, for SDS/nonionic surfactant mixtures.[5,38,39] However, in other mixed systems such as surfactant/alcohol mixtures, the impact on the self-assembly depends upon the alcohol structure and its location within the aggregate. This was discussed recently by Penfold et al.[40] for some model perfume molecules, where the more hydrophilic phenyl ethanol had little impact upon the self-assembly and the more hydrophobic molecules such as linalool promoted significant micellar growth.

b. Neutron Reflectivity. In their pioneering studies, Alargova and co-workers[10−13] also investigated the impact of multivalent counterions on the surface properties of SLES. However, this was done only on the basis of surface tension measurements. They derived an expression for the variation in surface tension

(38) Penfold, J.; Staples, E.; Tucker, I. *J. Phys. Chem. B* **2002**, *106*, 8891.
(39) Shiloach, A.; Blankstein, D. *Langmuir* **1998**, *14*, 7166.
(40) Penfold, J.; Tucker, I.; Green, A.; Grainger, D.; Jones, C.; Ford, G.; Roberts, C.; Hubbard, J.; Petkov, J.; Thomas, R. K.; Grillo, I. *Langmuir* **2008**, *24*, 12209.

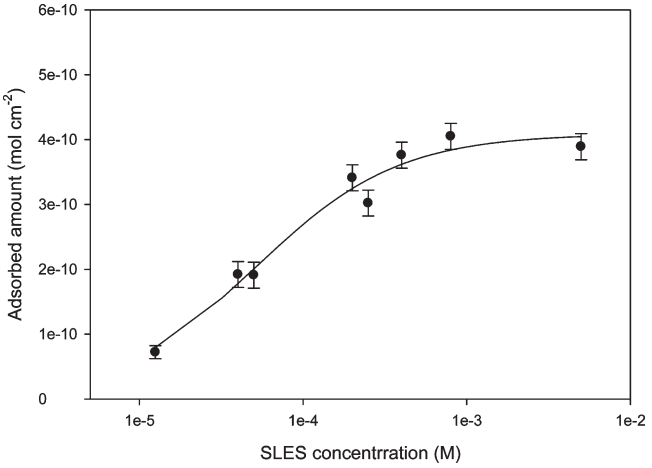

Figure 4. SLES adsorption isotherm (●); solid line is fit to Langmuir isotherm for parameters described in the text.

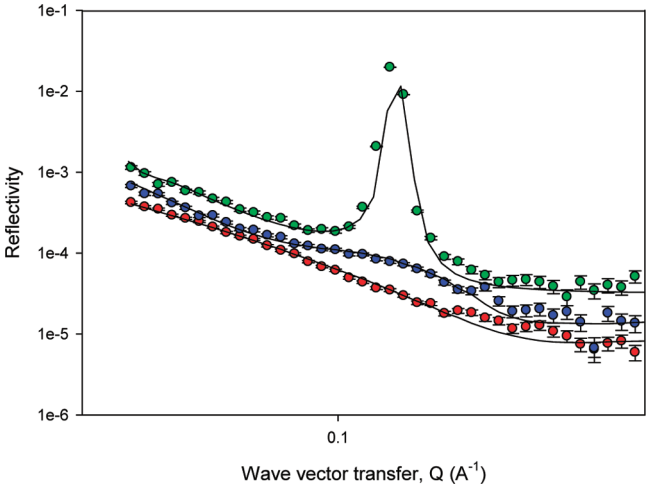

Figure 5. Reflectivity for 5 mM SLES/$AlCl_3$/NaCl, (red solid circle) 1.8/5.0 mM $AlCl_3$/NaCl, (blue solid circle) 1.9/4.6 mM, and (green solid circle) 2.1/3.75 mM. The different data are shifted vertically for clarity. The solid lines are model fits as described in the text.

with ionic strength, which took into account surfactant ion and counterion (both Al^{3+} and Na^+) adsorption; and this provided reasonable agreement with the surface tension variation. However, this approach is insensitive to the structure of the surface layer and in particular to any departure from simple monolayer adsorption. Penfold et al.[15] have recently reported that the addition of Ca^{2+} to SDBS and SDBS/nonionic surfactant mixtures promotes more complex surface structures and ultimately multilayer formation. This structural evolution is not evident in the associated surface tension data. Hence, we have used NR here to probe directly the impact of Al^{3+} and Ca^{2+} on the surface adsorption of SLES and SLES/$C_{12}E_{12}$ surfactant mixtures.

The adsorption properties of SLES have been relatively unexplored and hence some initial NR measurements were made in order to characterize the SLES adsorption at the air−water interface. Figure 4 shows the adsorption isotherm for SLES at the air−water interface obtained from the NR measurements, in the concentration range 10^{-5} to 5×10^{-3} M.

In this concentration range and in the absence of electrolyte, the NR data are consistent with a simple monolayer with a mean thickness, d, of ~22 ± 2 Å. The variation in the adsorption with surfactant concentration is broadly consistent with a Langmuir-type isotherm ($\Gamma = \Gamma_{max}c/(k_d + c)$, where Γ_{max} is 4.1×10^{-10} mol cm^{-2} and k_d is 5.7×10^{-5} mol), as illustrated by the solid line in Figure 4. The key model parameters from the analysis of the NR data, using the single monolayer of uniform thickness and where the adsorbed amount is calculated using eq 2, are summarized in Table S3 in the Supporting Information. The saturation adsorption is ~4.1×10^{-10} mol cm^{-2}, and the corresponding area/molecule is ~41 ± 2 Å^2. These values are similar to the closely related adsorption of SDS.[41]

Further NR measurements were made for 5 mM SLES in nrw, where the measurements were made for 5 mM d-SLES in nrw and for a 50/50 mol ratio of d-SLES/h-SLES in nrw, both in the presence of 10 mM $CaCl_2$. This provides, as demonstrated elsewhere,[42] a stringent test of the purity and consistency of the deuterium labeled SLES, d-SLES, compared to h-SLES; and within error, the two measurements give the same surface structure and adsorbed amount (see Table S4 in the Supporting Information).

(41) Lu, J. R.; Purcell, I. P.; Lee, E. M.; Simister, E. A.; Thomas, R. K.; Rennie, A. R.; Penfold, J. *J. Colloid Interface Sci.* **1995**, *174*, 4113.
(42) Simister, E. A.; Thomas, R. K.; Penfold, J.; Aveyard, R.; Binks, B. P.; Fletcher, P. D. I.; Lu, J. R.; Sokolowski, A. *J. Phys. Chem.* **1992**, *96*, 1383.

Table 2. Parameters for the 5 mM SLES/$AlCl_3$/NaCl Monolayer Model

$AlCl_3$/NaCl conc (mM)	d (±1 Å)	ρ_2 (±0.1 × 10^{-6} Å^{-2})	A (±2 Å^2)	Γ (±0.1 × 10^{-10} mol cm^{-2})
0.0/15.0	23	3.1	44	3.8
0.6/12.5	24	3.3	41	4.1
1.2/10.0	23	3.5	39	4.2
1.5/7.5	25	3.2	38	4.4
1.8/5.0	23	3.2	38	4.4

In the presence of multivalent counterions, the NR measurements were made predominantly for $AlCl_3$/NaCl mixed electrolytes, at surfactant concentrations of 1 and 5 mM, and for SLES and SLES/$C_{12}E_{12}$ mixtures. Figure 5 shows some typical reflectivity data for 5 mM SLES in the presence of $AlCl_3$/NaCl.

At the lowest $AlCl_3$ concentration in Figure 5 (1.8 mM), the data are consistent with a simple monolayer of uniform composition. The key model parameters in the monolayer region are summarized in Table 2, where Γ is the adsorbed amount in mol cm^{-2}. At an $AlCl_3$ concentration of 1.9 mM, the surface structure is more complex and an interference fringe is visible in the NR data at the intermediate Q values. This is now consistent with a bilayer structure at the interface, and the data are modeled by three layers. The key model parameters are summarized in Table 3. d_i and ρ_i are the thickness and scattering length density values for the three layers in the model, respectively, and d_1 and ρ_1 refer to the layer adjacent to the air phase.

At the higher $AlCl_3$ concentrations (2.0 mM and higher), the form of the reflectivity changes again, as shown in Figure 5 for 2.1 mM $AlCl_3$. The reflectivity is now dominated by a "Bragg peak", consistent with the formation of multilayers at the surface. The data were analyzed using the approach described earlier (eq 3), and the key model parameters are also summarized in Table 3. The number of bilayers is given by N, $d_1 + d_2$ is the bilayer thickness, and d_1, ρ_1 and d_2, ρ_2 are the thicknesses and scattering length densities, respectively, of the two layers comprising each bilayer.

Similar NR measurements were made at a surfactant concentration of 5 mM in the presence of $AlCl_3$/NaCl, but for SLES/$C_{12}E_{12}$ mixtures at surfactant compositions of 95/5, 93.5/6.5, 92/8, and 90/10 mol ratio SLES/$C_{12}E_{12}$. A broadly similar

Table 3. Parameters for the 5 mM SLES/$AlCl_3$/NaCl Multilayer Model[a]

$AlCl_3$/NaCl conc (mM)	d_1 (±1 Å)	ρ_1 (±0.1 × 10^{-6} Å^{-2})	d_2 (±1 Å)	ρ_2 (±0.1 ×10^{-6} Å^{-2})	d_3 (±1 Å)	ρ_3 (±0.1 × 10^{-6} Å^{-2})
1.9/4.6	25	3.2	22	0.3	21	0.9

$AlCl_3$/NaCl conc (mM)	d_1 (±0.2 Å)	ρ_1 (±0.1 × 10^{-6} Å^{-2})	d_2 (±0.2 Å)	ρ_2 (±0.1 × 10^{-6} Å^{-2})	N	ΔQ
2.0/4.0	25.2	3.6	25.2	2.0	40	0.05
2.1/3.75	25.2	3.4	25.2	1.0	40	0.05
2.4/2.5	25.2	3.5	25.2	0.7	40	0.05

[a] Note: ΔQ is the resolution, which comprises the instrumental resolution, ~0.04, convoluted with the mosaic spread of the lamellar stack at the interface. η (see eq 4) is ≳ 3000 Å in all the calculations made here.

evolution in the surface structure was observed with increasing $AlCl_3$ concentration, and the key model parameters are summarized in Table S5 in the Supporting Information. At low $AlCl_3$ concentrations, the surface structure is in the form of a monolayer, and with increasing $AlCl_3$ concentration there is a transition to bilayer and eventually to multilayer structures at the interface. With increasing amounts of $C_{12}E_{12}$, the transition from monolayer to bilayer/multilayer structures is shifted to higher $AlCl_3$ concentrations.

Further NR measurements were made for SLES and SLES/$C_{12}E_{12}$ mixtures in $AlCl_3$/NaCl mixed electrolyte at a lower total surfactant concentration of 1 mM. At this lower surfactant concentration, a much richer evolution in the surface structure was observed. This is illustrated in Figure 6 for 1 mM 95/5 mol ratio SLES/$C_{12}E_{12}$ in $AlCl_3$/NaCl.

The key model parameters for the data in this sequence of measurements, including the data shown in Figure 6, are summarized in Tables 4 and 5.

The data in Figure 6 are for $AlCl_3$ concentrations of 0.0, 0.24, 0.36, and 0.6 mM, and illustrate the more complex and detailed evolution in the structure of the surface layer. In the absence of $AlCl_3$, the data are consistent with a monolayer. Whereas for 0.24 mM $AlCl_3$ a pronounced interference fringe is visible at intermediate Q values and the data are consistent with a single bilayer at the interface, modeled as three layers as described earlier. For $AlCl_3$ concentrations of 0.36 mM and greater, the surface structure evolves into a surface multilayer structure with an increasing number of bilayers as the $AlCl_3$ concentration increases. For 0.36 mM $AlCl_3$, the data are consistent with three bilayers, and at 0.6 mM $AlCl_3$ there are ~20 bilayers at the surface. At the intermediate $AlCl_3$ concentration (not shown in the figure), the number of bilayers is ~10. Broadly similar data were obtained for 1 mM 90/10 SLES/$C_{12}E_{12}$ in $AlCl_3$/NaCl, except that the bilayer region extends over a wider range of $AlCl_3$ concentrations. The key model parameters from the analysis of the NR data are summarized in Table S6 in the Supporting Information.

From the quantitative analysis of the NR data for the variation in surface structure, a surface phase diagram can be constructed. This is shown in Figure 7a for 5 mM SLES/$C_{12}E_{12}$/$AlCl_3$/NaCl, and for 1 mM SLES/$C_{12}E_{12}$ in Figure 7b.

At a surfactant concentration of 5 mM and 100% SLES, there is a transition from a surface monolayer to a single bilayer structure as the $AlCl_3$ concentration increases, and a transition from the bilayer structure to the formation of surface multilayer structure at even higher $AlCl_3$ concentrations. With increasing amounts of $C_{12}E_{12}$, the surface monolayer structure increasingly dominates the surface behavior, and the more complex surface structures are only observed at the higher $AlCl_3$ concentrations. For solution compositions of SLES/$C_{12}E_{12}$ richer in $C_{12}E_{12}$ than 93.5/6.5 mol ratio and for $AlCl_3$ concentrations up to 3.0 mM, only surface monolayer adsorption is observed.

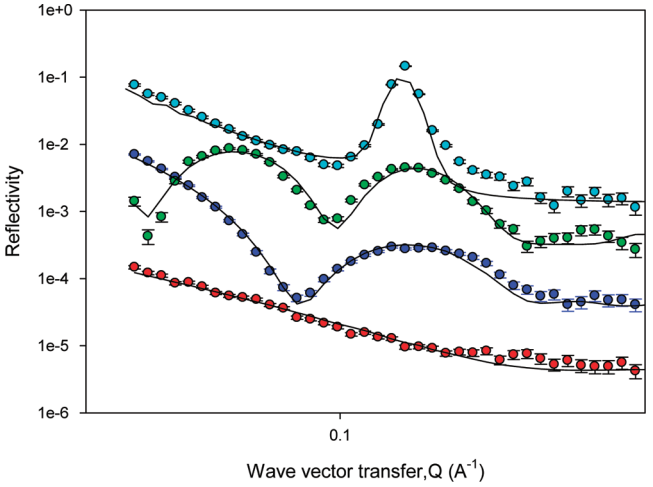

Figure 6. Reflectivity for 1 mM 95/5 mol ratio SLES/$C_{12}E_{12}$/$AlCl_3$/NaCl, (red solid circle) 0.0/3.0 mM $AlCl_3$/NaCl, (dark blue solid circle) 0.24/1.8 mM, (green solid circle) 0.36/1.2 mM, and (light blue solid circle) 0.6/0.0 mM. The different data are shifted vertically for clarity. The solid lines are model fits as described in the text.

At the lower surfactant concentration of 1 mM, a richer pattern of surface phase evolution is observed. Within the range of SLES/$C_{12}E_{12}$ compositions and $AlCl_3$ concentrations studied, the regions where surface bilayers and surface multilayers are formed are more extensive. Furthermore, the surface monolayer structures exist only in the absence of $AlCl_3$ and at the lowest $AlCl_3$ concentrations measured. There is an extensive region where the surface bilayer structures are found, and the extent of this region increases with increasing $AlCl_3$ concentration and with an increasing amount of $C_{12}E_{12}$ in the SLES/$C_{12}E_{12}$ mixture. The region where the surface multilayer structures are formed extend over a larger $AlCl_3$ concentration range for 100% SLES, and its extent decreases as the $C_{12}E_{12}$ content increases. At 1 mM surfactant concentration, the region where surface multilayer structures are observed has been subdivided into two separate regions, reflecting the more detailed evolution in the surface structure that is observed compared to 5 mM. At 5 mM surfactant concentration, the transition from a surface bilayer structure to the formation of surface multilayers is relatively abrupt, and once the surface multilayer structures form, the number of bilayers is immediately relatively large, > 20. In contrast, at 1 mM surfactant concentration, the surface multilayers that form at the higher $AlCl_3$ concentrations (blue data points in Figure 7b) also have a relatively large number of bilayers, 10−30. However, there is an intermediate region (green data points in Figure 7b) where the number of bilayers is finitely small and consists of only three bilayers.

This difference is also well illustrated in comparing the evolution in the NR data in Figures 5 and 6. At the highest $AlCl_3$

Table 4. Parameters for the 1 mM SLES/$AlCl_3$/NaCl Multilayer Model

$AlCl_3$/NaCl conc (mM)	d_1 (±1 Å)	ρ_1 (±0.1 × 10^{-6} Å^{-2})	d_2 (±1 Å)	ρ_2 (±0.1 × 10^{-6} Å^{-2})	d_3 (±1 Å)	ρ_3 (±0.1 × 10^{-6} Å^{-2})
0.12/2.4	19	3.7	13	1.0	33	3.1

$AlCl_3$/NaCl conc (mM)	d_1 (±0.2 Å)	ρ_1 (±0.1 × 10^{-6} Å^{-2})	d_2 (±0.2 Å)	ρ_2 (±0.1 × 10^{-6} Å^{-2})	N	ΔQ
0.24/1.8	19	2.5	27	0.1	3	0.1
0.3/1.5	19	2.5	27	0.1	3	0.1
0.6/0.0	24.5	1.2	24.5	0.4	30	0.05

Table 5. Parameters for the 1 mM 95/5 mol ratio SLES/$AlCl_3$/NaCl Multilayer Model

$AlCl_3$/NaCl conc (mM)	d_1 (±1 Å)	ρ_1 (±0.1 × 10^{-6} Å^{-2})	d_2 (±1 Å)	ρ_2 (±0.1 × 10^{-6} Å^{-2})	d_3 (±1 Å)	ρ_3 (±0.1 × 10^{-6} Å^{-2})
0.0/3.0	18	1.8				
0.24/1.8	22	3.6	15	1.1	24	0.9

$AlCl_3$/NaCl conc (mM)	d_1 (±0.2 Å)	ρ_1 (±0.1 × 10^{-6} Å^{-2})	d_2 (±0.2 Å)	ρ_2 (±0.1 × 10^{-6} Å^{-2})	N	ΔQ
0.36/1.2	14.8	2.7	28.5	0.3	3	0.1
0.48/0.6	24.3	2.6	24.3	1.2	10	0.15
0.6/0.0	24.3	2.6	24.3	1.2	20	0.1

concentrations, the NR data at both 1 and 5 mM surfactant concentration have a well-defined "Bragg" peak, characteristic of surface multilayer formation. However, the "Bragg" peak at 5 mM has a full-width-at-half-maximum, fwhm, of ~0.008 Å^{-1} compared to a value of ~0.012 Å^{-1} at 1 mM. This difference in fwhm has two contributing factors. The width of the "Bragg" peak is inversely proportional to the number of bilayers, and there is also a contribution of the instrumental resolution. There are two contributions to the apparent instrumental resolution, the actual instrumental resolution, which is ~4% in $\Delta Q/Q$, and the mosaic spread of the multilayer stack at the interface. In the data in Figures 5 and 6, the number of bilayers is ~40 at 5 mM and ~30 at 1 mM, but the apparent resolution has increased from 0.05 to 0.1 (see Tables 3 and 4), consistent with an increased mosaic spread. This increase in the mosaic spread can be considered as an increase in the orientational disorder at the interface. At lower $AlCl_3$ concentrations, the NR data for both surfactant concentrations are characterized by a well-defined interference fringe at intermediate Q values. This is characteristic of the formation of a thicker layer compared with a monolayer, but in the form of a single bilayer at the surface. At 1 mM surfactant concentration, the NR data at $AlCl_3$ concentrations intermediate between the bilayer and multilayer formation have a different form. It has two relatively broad interference fringes. As quantified in Table 4, this is consistent with a multilayer structure at the interface, but with a very small number (~3) of bilayers.

In solution, the addition of multivalent counterions Ca^{2+} and Al^{3+} promotes significant growth in the SLES micelle size and, ultimately, in the transition to planar multilayer structures and precipitation. This growth is now attributed to the strong binding of the Ca^{2+} or Al^{3+} counterions to the micellar surface to reduce local curvature. The effect of the Al^{3+} counterions was more significant than that of Ca^{2+} counterions, where the SLES/Al^{3+} trimer formation has a greater impact than the SLES/Ca^{2+} dimer formation. At the surface, where only the impact of Al^{3+} was studied, the strong SLES/Al^{3+} complexation results in the transition from a simple adsorbed monolayer to bilayer and multilayer surface structures at the interface. As quantified in Tables 2 and 3, for 5 mM SLES in $AlCl_3$/NaCl, the increasing addition of $AlCl_3$ results in a reduction in the mean area/molecule. Furthermore, associated with this reduction in the area/molecule, the SLES/Al^{3+} trimer complex formation at the interface will also reduce the surface charge. Both factors contribute to the change in the surface structure from a simple monolayer to multiple layers at the interface. This is directly analogous to what was previously reported by Penfold et al.[15] for the SDBS/nonionic surfactant mixture, where surface multilayer formation was induced by the addition of Ca^{2+} counterions. In that study, the SDBS-6 isomer used means that the SDBS was essentially a short dialkyl chain ionic surfactant. Surface multilayer formation has been observed in other longer alkyl chain dialkyl chain cationic surfactants, but at much higher surfactant concentrations.[34−45] It has also been observed at relatively low surfactant concentrations, but in that case with the addition of much higher amounts of electrolyte.[46] This is the first reported observation in a single alkyl chain surfactant at relatively low surfactant and electrolyte concentrations. The strong SLES/Al^{3+} complexation and trimer formation is the major factor which promotes these more complex surface structures.

The addition of a nonionic cosurfactant with a large EO headgroup was shown to suppress the micellar growth induced by the multivalent counterions, due to the steric hindrance of the bulky headgroup which inhibits dimer and trimer complex formation. The addition of $C_{12}E_{12}$ suppresses the transition from monolayer to multilayer adsorption as the increasing amount of $C_{12}E_{12}$ inhibits or disturbs SLES/Al^{3+} complex formation, due to the steric hindrance of the larger EO_{12} headgroup. The impact is is different at 5 and 1 mM.

We have observed that the NR data at 1 mM show a richer evolution in the surface phase behavior than at 5 mM. Furthermore, it is evident that, analogous to the solution behavior, the strong SLES/Al^{3+} complexation is the major driving force for the transition from a simple monolayer adsorption to multilayer adsorption. It was shown in the micellar growth with the addition of Al^{3+} that the onset of growth is strongly correlated with ξ and occurs when $\xi < 1.0$. When $\xi = 1.0$, $C_s - \text{cmc} = 3C_{Al}$, the number of surfactant ions is equal to the number of Al^{3+} ions times their charge. If we assume that the point at which multilayer formation at the interfaces starts is the point at which the surface adsorption starts to effectively diverge, then this also

(43) Li, Z. X.; Waller, A.; Thomas, R. K.; Rennie, A. R.; Webster, J. R. P.; Penfold, J.; heenan, R. K.; Cubitt, R. *J. Phys. Chem. B* **1999**, *103*, 1080.
(44) Li, Z. X.; Lu, J. R.; Thomas, R. K.; Waller, A.; Penfold, J.; Webster, J. R. P.; Rennie, A. R. *Langmuir* **2001**, *17*, 5858.
(45) McGillivray, D. J.; Thomas, R. K.; Rennie, A. R.; Penfold, J; Sivia, D. S. *Langmuir* **2003**, *19*, 7719.
(46) Penfold, J.; Staples, E.; Tucker, I.; Thomas, R. K. *Langmuir* **2004**, *20*, 2265.

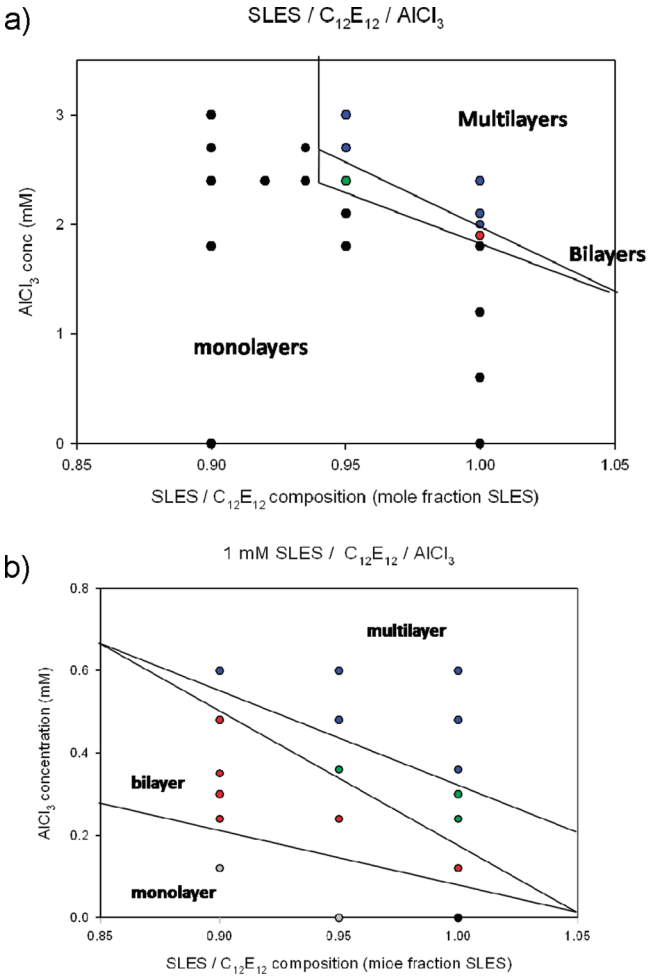

Figure 7. Surface phase diagram for (a) 5 mM SLES/$C_{12}E_{12}$/$AlCl_3$/NaCl and (b) 1 mM SLES/$C_{12}E_{12}$/$AlCl_3$/NaCl.

correlates with a value of ξ of <1.0, at both 1.0 and 5.0 mM SLES concentration.

Alargova and co-workers[10−13] measured the variation in surface tension with ξ and showed that the variation correlated with the divergence in the micellar size (as described by the hydrodynamic radius from light scattering). That is, below $\xi = 1.0$, the surface tension was constant. For $\xi > 1.0$, they used the expression

$$d\sigma = -kT\Gamma_s\left(d \ln \mathrm{cmc} + \theta_N d \ln C_{NB} + \frac{\theta_A}{3} d \ln C_{AB}\right) \quad (8)$$

where Γ_s is the surfactant adsorption, $\theta_N = \Gamma_N/\Gamma_s$ and $\theta_A = \Gamma_A/\Gamma_s$ are the relative adsorption of Na and Al ions, respectively, and C_{NB} and C_{AB} are their respective bulk concentrations to calculate the variation of σ with ξ. It provided good agreement with the variation with ξ at constant Al^{3+} concentration, and only moderate agreement at constant ionic strength. Alargova and co-workers[10−13] also measured the variation in surface potential, ΔV, with ξ and demonstrated a gradual decrease in ΔV with decreasing ξ, but observed no discontinuity in the ΔV dependence at $\xi \sim 1.0$. The surface potential and surface tension data are evidently insensitive to the onset of surface multilayer formation, although they do strongly support the trend toward charge neutrality at $\xi = 1.0$.

By analogy with the work of Alargova co-workers[10−13] on self-assembly, the main driving force for the transition from a simple monolayer to the more complex multilayer structures at the interface is the strong SLES/Al^{3+} complexation. A nonionic cosurfactant, with a sufficiently large headgroup, disrupts that complex formation. Although the correlation with the value of ξ points to charge neutrality being an important factor, it is not a sufficient criterion. The addition of NaCl, at an equivalent ionic strength, does not promote the transition from a monolayer to multilayer structures in this system. The SLES ion/Al^{3+} complex formation also results in a significant reduction in the area per molecule of the SLES ions associated with the Al^{3+} ion. This results in a much greater intermolecular alkyl chain interaction, and we postulate that is an important factor in promoting the multilayer formation at the interface. The relative importance of the alkyl chain interaction is reinforced by other observations on related systems. For example, Penfold et al.[46] observed that the addition of KBr promoted the formation of surface multilayer structures in the dialkyl chain cationic surfactant, dihexadecyl dimethyl ammonium bromide, DHDAB, at relatively low surfactant concentrations.

Hence, the NR results provide a new insight into the response of the surface adsorption to the addition of multivalent counterions and illustrate a dramatic change in the surface structure for $\xi < 1.0$. The data reveal a complex evolution from monolayer to bilayer to multilayer structures at the interface which are strongly dependent upon the surfactant concentration and counterion type and concentration. Furthermore, they illustrate and confirm the ability of the nonionic cosurfactant with a large headgroup to disrupt the strong complex formation that determines the structural evolution, as was observed in also in bulk solution. Substantial developments in the theoretical treatment of surfactant adsorption are required in order to further quantify and explain these observed trends and are currently underway.[47]

Summary

The NR and SANS measurements have provided a detailed and quantified insight into the impact of multivalent counterions, and especially Al^{3+}, on the surface adsorption and solution self-assembly properties of the anionic surfactant SLES and the anionic/nonionic surfactant mixture of SLES/$C_{12}E_{12}$.

In solution, the addition of multivalent counterions promotes substantial micellar growth, which has now been quantified and correlated with the point at which counterions are in excess. At low surfactant concentrations, the substantial micellar growth results ultimately in the formation of planar (lamellar) structures and eventually precipitation. The addition of a nonionic cosurfactant with a large EO headgroup suppresses the micellar growth as the steric hindrance of the nonionic headgroup disrupts the strong SLES/counterion dimer or trimer complex formation responsible for the growth.

At the surface, we have for the first time observed and quantified the impact of multivalent counterions on the surface adsorption behavior of SLES and SLES/$C_{12}E_{12}$ mixtures. The same strong SLES/counterion complex formation now drives a transition from a simple monolayer to surface multilayer formation. The monolayer to multilayer transition is also associated with multivalent counterion excess. Furthermore, the steric hindrance imposed by the nonionic cosurfactant inhibits or shifts that transition to higher multivalent counterion concentrations. At surfactant concentrations just above the cmc, a more subtle

(47) Morgan, C.; Breward, C.; Howell, P.; Thomas, R. K.; Penfold, J. Private communication.

and complex evolution in surface structure is observed and is not explained by existing theoretical treatments.

The results presented build substantially upon the pioneering work of Alargova and co-workers[10−13] in this area, and especially in characterizing the impact of Al^{3+} ions on the surface adsorption behavior. The results provide an important insight into how multivalent counterions and a nonionic cosurfactant can be used to manipulate both the solution self-assembly and the surface properties in surfactant systems. In solution, the manipulation and control of micellar growth and size provides the opportunity to tailor rheological properties and to manipulate solubilization patterns. At the interface, the formation of multilayer structures at the interface is also associated with extreme and persistant wetting patterns, and offers potential applications in soft lubrication and in the efficient delivery of benefit agents to surfaces or interfaces.

Acknowledgment. We acknowledge the provision of neutron beam time on LOQ and SURF at ISIS and on D11 at the ILL, and the assistance of the instrument scientists John Webster, Arwel Hughes, and Sarah Rogers at ISIS and beamline engineer David Bowyer at the ILL.

Supporting Information Available: Model parameters from the analysis of the SLES/$C_{12}E_{12}$ SANS data and the NR data. This material is available free of charge via the Internet at http://pubs.acs.org.